Modeling of Electroosmotic Flow and Capillary Electrophoresis with the Joule Heating Effect: The Nernst−Planck Equation versus the Boltzmann Distribution

G. Y. Tang, C. Yang,* C. J. Chai, and H. Q. Gong

School of Mechanical and Production Engineering, Nanyang Technological University, Republic of Singapore 639798

Received May 9, 2003. In Final Form: August 29, 2003

Joule heating is present in electrokinetic transport phenomena, which are widely used in microfluidic systems. In this paper, a rigorous mathematical model is developed to describe the Joule heating and its effects on electroosmotic flow and mass species transport in microchannels. The proposed model includes the Poisson equation, the modified Navier−Stokes equation, and the conjugate energy equation (for the liquid solution and the capillary wall). Specifically, the ionic concentration distributions are modeled using (i) the general Nernst−Planck equation and (ii) the simple Boltzmann distribution. The relevant governing equations are coupled through the temperature-dependent solution dielectric constant, viscosity, and thermal conductivity, and, hence, they are numerically solved using a finite-volume-based CFD technique. The applicability of the Nernst−Planck equation and the Boltzmann distribution in the electroosmotic flow with Joule heating has been discussed. The results of the time and spatial development for both the electroosmotic flow field and the Joule heating induced temperature field are presented. It is found that the presence of the Joule heating can result in significantly different electroosmotic flow and mass species transport characteristics.

I. Introduction

Electroosmosis refers to liquid flow induced by an applied external electric field along electrostatically charged surfaces. It is one of the basic electrokinetic phenomena and has been found in a variety of applications such as dewatering of waste sludge and removing heavy metal ions from soils for environmental remediation.[1] In addition, the electroosmosis is being extensively used in lab-on-a-chip (or BioMEMS) technology as a transporting mode to manipulate liquids, such as pumping, valving, mixing, and splitting, and to deliver solute samples of nanovolumes in microfluidics used for chemical and biological analyses and medical diagnoses.[2,3] In the literature, a great deal of information has been generated on electroosmotic flow (EOF) in microcapillaries of various geometric domains, such as cylindrical capillary,[4,5] annulus,[6] elliptical pore,[7] slit parallel plate,[8] rectangular microchannel,[9] and T-shaped and Y-shaped microchannel structures.[10] Moreover, many studies have been reported on sample transport and mixing[11−13] based on capillary electrophoresis (CE).

The motivation of this work can be attributed to two factors. First, all aforementioned studies of the EOF and CE have neglected the Joule heating effect. It is well-known that Joule heating is generated when an electric field is applied across conductive liquids. Such Joule heating not only can cause a temperature increase but also may create a temperature gradient. The change of the liquid temperature and the presence of a temperature gradient would have an impact on the EOF and CE.[14−16] Previous studies have amply demonstrated that the effects of Joule heating can result in a strong dispersion, leading to a low column separation efficiency, reduction of analysis resolution, and even loss of injected samples. Further, the temperature rise can give rise to the decomposition of thermally labile samples and formation of gas bubbles as well. Recently, Swinney and Bornhop[17] measured the Joule heating in a chip-scale CE by using a novel picoliter volume interferometer. Their results showed that the Joule heating effect on the CE has been underestimated and, hence, there is a need to reexamine the theoretical modeling. Nonetheless, previous studies reported on the Joule heating effect are either empirical or based on simplified theories. To date, very few studies have been reported on the Joule heating and its effects on the EOF and CE on the basis of rigorous mathematical models, which not only can offer a quantitative estimate of the

* To whom correspondence should be addressed. Tel.: +65-6790-4883. Fax: +65-6791-1859. E-mail: mcyang@ntu.edu.sg.

(1) Masliyah, J. H. *Electrokinetic Transport Phenomena*; AOSTRA Technical Publication Series No. 12; AOSTRA: Edmonton, 1994.
(2) Harrison, D. J.; Fluri, K.; Seiler, K.; Fan, Z.; Effenhauser, C. S.; Manz, A. *Science* **1993**, *261*, 895−897.
(3) Bousse, L.; Cohen, C.; Nikiforov, T.; Chow, A.; Kopf-Sill, A. R.; Dubrow, R.; Parce, J. W. *Annu. Rev. Biophys. Biomol. Struct.* **2000**, *29*, 155−181.
(4) Keh, H. J.; Tseng, H. C. *J. Colloid Interface Sci.* **2002**, *242*, 450−459.
(5) Kang, Y. J.; Yang, C.; Huang, X. Y. *Int. J. Eng. Sci.* **2002**, *40*, 2203−2221.
(6) Kang, Y. J.; Yang, C.; Huang, X. Y. *J. Colloid Interface Sci.* **2002**, *253*, 285−294.
(7) Hsu, J. P.; Kao, C. Y.; Tseng, S.; Chen, C. J. *J. Colloid Interface Sci.* **2002**, *248*, 176−184.
(8) Yang, C.; Ng, C. B.; Chan, V. *J. Colloid Interface Sci.* **2002**, *248*, 524−527.
(9) Yang, C.; Li, D. *J. Colloid Interface Sci.* **1997**, *194*, 95−107.
(10) Patankar, N. A.; Hu, H. H. *Anal. Chem.* **1998**, *70*, 1870−1881.
(11) Ermakov, S. V.; Jacobson, S. G.; Ramsey, J. M. *Anal. Chem.* **1998**, *70*, 4494−4504.
(12) Jeon, N. L.; Dertinger, S. K. W.; Chiu, D. T.; Choi, I. S.; Stroock, A. D.; Whitesides, G. M. *Langmuir* **2000**, *16*, 8311−8316.
(13) Erickson, D.; Li, D. *Langmuir* **2002**, *18*, 1883−1892.
(14) Grushka, E.; McCormick, R. M.; Kirkland, J. J. *Anal. Chem.* **1989**, *61*, 241−246.
(15) Knox, J. H.; McCormack, K. A. *Chromatographia* **1994**, *38*, 207−214.
(16) Bosse, M. A.; Arce, P. *Electrophoresis* **2000**, *21*, 1026−1033.
(17) Swinney, K.; Bornhop, D. J. *Electrophoresis* **2002**, *23*, 613−620.

10.1021/la0301994 CCC: $25.00
Published on Web 11/21/2003

Joule heating but also can lead to the optimum design and precise control of BioMEMS.

Second, the ionic concentration distributions are assumed to follow the Boltzmann distribution in the aforementioned studies. Strictly speaking, the Boltzmann distribution is applicable only when the system is in the thermodynamic equilibrium state.[1] If a liquid flow exists, the ionic concentration distributions may be affected by the presence of the fluid motion.[18] Furthermore, because the mass diffusivity of ions can be temperature-dependent, the presence of the temperature gradient resulted from the Joule heating may also cause the ionic concentration distributions to deviate from the Boltzmann distribution. Therefore, the general Nernst−Planck equation should be used to describe the ionic concentration distribution distributions in these situations.[18,19] It is noted that Yang et al.[20] used the Nernst−Planck equation to study the temporal and spatial development of the EOF in a two-parallel-plate microchannel, but they neither included the Joule healing in their models nor provided quantitative conditions under which the Boltzmann distribution can be assumed. Recently, Erickson and Li[21] analyzed the electroviscous effect on pressure-driven microchannel flow with a heterogeneous surface, and the Nernst−Planck equation was included to account for the non-Boltzmann distribution due to electrokinetic heterogeneity. Again, the Joule heating was not considered in their model development.

In this work, a mathematical model for the EOF and CE with Joule heating is developed. The model includes the Poisson equation for the electric double layer (EDL) potential profile, the modified Navier−Stokes equation for the EOF velocity field, and the energy equation for the temperature field created by Joule heating. Specifically, the ionic concentration distributions are modeled using (i) the general Nernst−Planck equation to account for the influence of the fluid flow and the temperature field, and (ii) the simple Boltzmann equation. All relevant equations are coupled through temperature-dependent parameters, such as the electrolyte dielectric constant, liquid viscosity, ion diffusion coefficient, thermal and electric conductivities, and so forth. These coupled equations are numerically solved using a finite-volume-based CFD technique. Furthermore, a comparison has been made for the results of the ionic concentration distributions and the EOF and temperature fields obtained from the Nernst−Planck equation and the Boltzmann equation. In addition, sample-species transport is investigated by numerically solving the mass-transport equation, taking into account of the temperature-dependent mass diffusivity and electrophoresis mobility. The transient temperature development in the capillary and its effect on the velocity of EOF and the sample transport are also studied.

II. Problem Formulation

The model presented in this study includes the Poisson equation governing the EDL potential distributions, the modified Navier−Stokes equation describing the motion of liquid driven by electrokinetic body forces, and the energy equation governing the temperature field due to Joule heating, while the ionic concentration distributions are either governed by the Nernst−Planck equation or described by the Boltzmann distribution. Therefore, two sets of equations are formulated to describe the electrokinetic transport phenomenon in a microchannel with consideration of the Joule heating effect. Moreover, in view of the fact that EOF is mainly used for delivering and separating chemical or biological samples, the mass species transport equation is, therefore, included in the model development to examine the Joule heating effect. A cylindrical microcapillary, which is widely used in bioengineering processes such as CE and high-performance liquid chromatography (HPLC), is chosen as the computational domain in the present study.

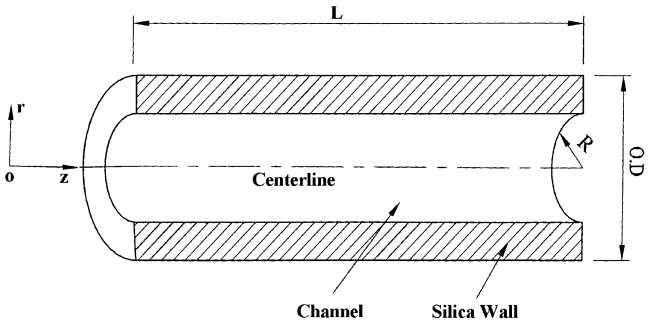

Figure 1. Schematic diagram of the circular capillary with a cylindrical coordinate system.

II.A. Electrical Potential Distribution. Consider an EOF in a cylindrical microcapillary with inner radius, R, and length, L, as shown in Figure 1. When a solid surface is in contact with a polar medium, the surface usually becomes charged.[22] Due to electrostatic interactions, both co-ions and counterions are preferentially redistributed near the charged surface, leading to the formation of an EDL. According to the theory of electrostatics,[22] the electrical potential distributions $\psi(r, z)$ is governed by the Poisson equation,

$$\frac{1}{r}\frac{\partial}{\partial r}\left[r\epsilon(T)\frac{\partial\psi}{\partial r}\right] + \frac{\partial}{\partial z}\left[\epsilon(T)\frac{\partial\psi}{\partial z}\right] = -\frac{\rho_e}{\epsilon_0} \quad (1)$$

where ϵ_0 is the permittivity of the vacuum and ϵ is the dielectric constant of the electrolyte and is considered as a function of the temperature, $\epsilon(T) = 305.7\ \exp(-T/219)$ (assumed the same as water). For a symmetric electrolyte, the local net charge density, ρ_e is given by

$$\rho_e(r, z) = \sigma e(n_+ - n_-) \quad (2)$$

where n_+ and n_- are the concentrations of the cations and anions, respectively, σ is the valence of the ions of the electrolyte, and e is the fundamental charge. Substituting eq 2 into eq 1, we can obtain

$$\frac{1}{r}\frac{\partial}{\partial r}\left[r\epsilon(T)\frac{\partial\psi}{\partial r}\right] + \frac{\partial}{\partial z}\left[\epsilon(T)\frac{\partial\psi}{\partial z}\right] = -\frac{\sigma e(n_+ - n_-)}{\epsilon_0} \quad (3)$$

Introducing nondimensional parameters,

$$\bar{r} = \frac{r}{R} \qquad \bar{z} = \frac{z}{R} \qquad \bar{\psi} = \frac{\sigma e\psi}{k_b T} \qquad \bar{\epsilon} = \frac{\epsilon(T)}{\epsilon_{ref}}$$
$$\bar{n}_+ = \frac{n_+}{n_0} \qquad \bar{n}_- = \frac{n_-}{n_0} \quad (4)$$

(18) Yang, C.; Li, D.; Masliyah, J. H. *Int. J. Heat Mass Transfer* **1998**, *41*, 4229−4249.
(19) Lyklema, J. *Fundamentals of Interface and Colloid Science: Solid−Liquid Interfaces*; Academic Press: San Diego, 1995; Vol. 2.
(20) Yang, R. J.; Fu, L. M.; Hwang, C. C. *J. Colloid Interface Sci.* **2001**, *24*, 173−179.
(21) Erickson, D.; Li, D. *Langmuir* **2002**, *18*, 8949−8959.
(22) Hunter, R. J. *Zeta Potential in Colloid Science: Principles and Applications*; Academic Press: New York, 1981.

we can express eq 3 in dimensionless form as

$$\frac{1}{\bar{r}}\frac{\partial}{\partial \bar{r}}\left[\bar{r}\bar{\epsilon}\frac{\partial \bar{\psi}}{\partial \bar{r}}\right] + \frac{\partial}{\partial \bar{z}}\left[\bar{\epsilon}\frac{\partial \bar{\psi}}{\partial \bar{z}}\right] = -\frac{(\kappa R)^2}{2}(\bar{n}_+ - \bar{n}_-) \qquad (5)$$

where ϵ_{ref} is the dielectric constant of the electrolyte at room temperature (i.e., $T_0 = 298$ K) and it is chosen to be 78.5 in all computations unless specified otherwise, k_b is the Boltzmann constant, n_0 is the bulk ionic number concentration in the electrolyte solution, and T is the absolute temperature. $\kappa = (2n_0\sigma^2e^2/\epsilon_{ref}\epsilon_0k_bT)^{1/2}$ is the Debye−Hückel parameter, and its reciprocal represents the EDL thickness. In the literature, κR is called the electrokinetic radius, and it characterizes the ratio of the geometric dimension to the EDL thickness, representing the relative contribution of the EDL effect.

II.B. Modified Navier−Stokes Equations. Different from the conventional pressure-driven flows, the driving force of EOF is due to the interaction between the net charge density in the EDL regime and the applied electric field. Therefore, the Navier−Stokes equations, including the continuity equation and the momentum equation describing a laminar, incompressible, unsteady flow of an electrolyte with temperature-dependent viscosity, are modified to

Continuity Equation

$$\frac{1}{r}\frac{\partial}{\partial r}(rv_r) + \frac{\partial v_z}{\partial z} = 0 \qquad (6)$$

Momentum Equations

$$\rho\left[\frac{\partial v_z}{\partial t} + v_r\frac{\partial v_z}{\partial r} + v_z\frac{\partial v_z}{\partial z}\right] = -\frac{\partial p}{\partial z} + \frac{1}{r}\frac{\partial}{\partial r}\left[r\mu(T)\frac{\partial v_z}{\partial r}\right] + \frac{\partial}{\partial z}\left[\mu(T)\frac{\partial v_z}{\partial z}\right] + \rho_e\left(E - \frac{\partial \psi}{\partial z}\right) \qquad (7a)$$

$$\rho\left[\frac{\partial v_r}{\partial t} + v_r\frac{\partial v_r}{\partial r} + v_z\frac{\partial v_r}{\partial z}\right] = -\frac{\partial p}{\partial r} + \frac{\partial}{\partial r}\left[\frac{\mu(T)}{r}\frac{\partial (rv_r)}{\partial r}\right] + \frac{\partial}{\partial z}\left[\mu(T)\frac{\partial v_r}{\partial z}\right] - \rho_e\frac{\partial \psi}{\partial r} \qquad (7b)$$

where v_z and v_r are the velocity of EOF in the axial and radial directions, respectively, t is the time, ρ is the mass density of the solution and is assumed as a constant, p is the dynamic pressure, E is the strength of an externally applied electric field along the axial direction, and μ is the temperature-dependent viscosity of the electrolyte solution, $\mu(T) = 2.761 \times 10^{-6}\exp(1713/T)$ (assumed the same as water). These governing equations can be nondimensionalized by introducing the following dimensionless parameters:

$$\bar{v}_z = \frac{v_z}{U_{ref}} \qquad \bar{v}_r = \frac{v_r}{U_{ref}} \qquad \bar{P} = \frac{p}{\rho U_{ref}^2} \qquad \bar{t} = \frac{U_{ref}t}{R}$$
$$\bar{\mu} = \frac{\mu(T)}{\mu_{ref}} \qquad Re = \frac{\rho R U_{ref}}{\mu_{ref}} \qquad (8)$$

where U_{ref} and μ_{ref} are the reference velocity and dynamic viscosity, respectively. Re is the Reynolds number representing the ratio of the inertia force to the viscous force. Then, eqs 6 and 7 in dimensionless form are expressed as

$$\frac{1}{\bar{r}}\frac{\partial}{\partial \bar{r}}(\bar{r}\bar{v}_r) + \frac{\partial \bar{v}_z}{\partial \bar{z}} = 0 \qquad (9)$$

$$\frac{\partial \bar{v}_z}{\partial \bar{t}} + \bar{v}_r\frac{\partial \bar{v}_z}{\partial \bar{z}} + \bar{v}_z\frac{\partial \bar{v}_z}{\partial \bar{z}} = -\frac{\partial \bar{p}}{\partial \bar{z}} + \frac{1}{Re}\left\{\frac{1}{\bar{r}}\frac{\partial}{\partial \bar{r}}\left[\bar{r}\bar{\mu}\frac{\partial \bar{v}_z}{\partial \bar{r}}\right] + \frac{\partial}{\partial \bar{z}}\left[\bar{\mu}\frac{\partial \bar{v}_z}{\partial \bar{z}}\right]\right\} + A(\bar{n}_+ - \bar{n}_-) - B\frac{\partial \bar{\psi}}{\partial \bar{z}}(\bar{n}_+ - \bar{n}_-) \qquad (10a)$$

$$\frac{\partial \bar{v}_r}{\partial \bar{t}} + \bar{v}_r\frac{\partial \bar{v}_r}{\partial \bar{r}} + \bar{v}_z\frac{\partial \bar{v}_r}{\partial \bar{z}} = -\frac{\partial \bar{p}}{\partial \bar{r}} + \frac{1}{Re}\left\{\frac{\partial}{\partial \bar{r}}\left[\frac{\bar{\mu}}{\bar{r}}\frac{\partial (\bar{r}\bar{v}_r)}{\partial \bar{r}}\right] + \frac{\partial}{\partial \bar{z}}\left[\bar{\mu}\frac{\partial \bar{v}_r}{\partial \bar{z}}\right]\right\} - B\frac{\partial \bar{\psi}}{\partial \bar{r}}(\bar{n}_+ - \bar{n}_-) \qquad (10b)$$

$$A = \frac{R\sigma e n_0 E}{\rho U_{ref}^2} \qquad B = \frac{n_0 k_b T_0}{\rho U_{ref}^2} \qquad (10c)$$

where A and B are dimensionless parameters and physically they represent the ratios of ionic electrostatic energy to kinetic energy and thermal energy to kinetic energy, respectively.

II.C. Energy Equation. The transient energy equation taking account of the temperature-dependent thermal conductivity and heat source can be expressed as

$$\rho c_p\left(\frac{\partial T}{\partial t} + v_r\frac{\partial T}{\partial r} + v_z\frac{\partial T}{\partial z}\right) = \frac{1}{r}\frac{\partial}{\partial r}\left[rk_l(T)\frac{\partial T}{\partial r}\right] + \frac{\partial}{\partial z}\left[k_l(T)\frac{\partial T}{\partial z}\right] + \Phi + \dot{q} \qquad (11)$$

where c_p and $k_l(T)$ are the specific heat capacity and the temperature-dependent thermal conductivity of the electrolyte, respectively. The heat source consists of viscous dissipation (Φ) and Joule heating ($\dot{q}$). The heat generation due to viscous dissipation can be expressed as

$$\Phi = \mu(T)\left\{2\left[\left(\frac{\partial v_r}{\partial r}\right)^2 + \left(\frac{\partial v_z}{\partial z}\right)^2\right] + \left(\frac{\partial v_r}{\partial z} + \frac{\partial v_z}{\partial r}\right)^2\right\} \qquad (12)$$

According to the Ohm's law, the heat generation due to Joule heating is given by where I is the electrical current

$$\dot{q} = I^2/\lambda \qquad (13)$$

density in the electrolyte and λ is the electrical conductivity of the electrolyte. According to Weast et al.,[23] λ is temperature-dependent and can be expressed as

$$\lambda = \lambda_+(T)\eta_+ + \lambda_-(T)\eta_- \qquad (14a)$$

$$\lambda_+(T) = \lambda_{+0} + 0.025\lambda_{+0}(T - 298) \qquad (14b)$$

$$\lambda_-(T) = \lambda_{-0} + 0.025\lambda_{-0}(T - 298) \qquad (14c)$$

Here, $\lambda_+(T)$ and $\lambda_-(T)$ are the electical conductivities of the cations and anions of the electrolyte at temperature T, respectively, λ_{+0} and λ_{-0} are the electrical conductivities of the cations and anions of the electrolyte at room temperature, respectively, and η_+ and η_- denote the mole concentration of the cations and anions of the electrolyte. In this situation, the electrical current density includes two parts; one is due to the applied electric field imposing on the conductive solution ($E\lambda$), and the other is due to the net charged density moving with the fluid ($v_z\rho_e$). Therefore,

(23) Weast, R.; Astle, M. J.; Beyer, W. H. *CRC Handbook of Chemistry and Physics*; CRC Press, Inc.: Boca Raton, 1986.

the electrical current density, I, can be further expressed as

$$I = v_z\rho_e + E\lambda \tag{15}$$

Substituting eq 15 into eq 13 gives the expression for the Joule heating rate as

$$\dot{q} = (v_z\rho_e + E\lambda)^2/\lambda \tag{16}$$

The above governing equations can be nondimensionalized by introducing the following dimensionless parameters:

$$\bar{k}_l = \frac{k_l(T)}{k_{ref}} \qquad \bar{T} = \frac{T - T_{ref}}{T_0 - T_{ref}} \qquad Re = \frac{\rho R U_{ref}}{\mu_{ref}} \qquad Pr = \frac{\nu_{ref}}{k_{ref}/\rho C_p} \tag{17}$$

where k_{ref} and T_{ref} are the reference thermal conductivity and temperature, respectively, ν_{ref} is the reference kinematic viscosity, and Pr is the Prandtl number. Therefore, the energy equation in dimensionless form can be expressed as

$$\frac{\partial\bar{T}}{\partial\bar{t}} + \bar{v}_r\frac{\partial\bar{T}}{\partial\bar{r}} + \bar{v}_z\frac{\partial\bar{T}}{\partial\bar{z}} = \frac{1}{Pr\ Re}\left[\frac{1}{\bar{r}}\frac{\partial}{\partial\bar{r}}\left(\bar{r}\bar{k}_l\frac{\partial\bar{T}}{\partial\bar{r}}\right) + \frac{\partial}{\partial\bar{z}}\left(\bar{k}_l\frac{\partial\bar{t}}{\partial\bar{z}}\right)\right] + \bar{\Phi} + \bar{q} \tag{18}$$

$$\bar{\Phi} = \frac{\Phi}{\rho c_p U_{ref}(T_0 - T_{ref})/R} \tag{19}$$

$$\bar{q} = \frac{\dot{q}}{\rho c_p U_{ref}(T_0 - T_{ref})/R} \tag{20}$$

It should be pointed out here that, different from thermal convection in large-sized channels, for creeping low Reynolds number microchannel flows, the Reynolds number is no longer the governing parameter anymore. The controlling parameter become thermal Péclet number (i.e., $Pr\ Re$).

II.D. Ionic Concentration Distributions. In this study, the ionic concentration distributions are described using two models, namely, the Nernst−Planck equation and the Boltzmann distribution.

Nernst−Planck Equation. In general, the ionic concentration distributions n_i in the presence of flow and temperature fields are described by the Nernst−Planck equation,[19]

$$\frac{\partial n_i}{\partial t} + \vec{V}\cdot\nabla n_i = \nabla\cdot[D_i(T)\nabla n_i] + \nabla\cdot\left[\frac{n_i\sigma_i e D_i(T)}{k_b T}\nabla(\psi)\right] \tag{21}$$

In this equation, $\vec{V}$ is the velocity vector, n_i is the concentration of either cations (n_+) or anions (n_-), and $D_i(T)$ is the temperature-dependent diffusion coefficient of the corresponding ions. According to Weast et al.,[23] $D_i(T)$ can be expressed as

$$D_i(T) = D_{i0} + 0.025D_{i0}(T - 298) \tag{22}$$

where D_{i0} is the diffusion coefficient of corresponding ions at room temperature. Under the cylindrical coordinate system, eq 21 can be further expanded as

$$\frac{\partial n_i}{\partial t} + v_r\frac{\partial n_i}{\partial r} + v_z\frac{\partial n_i}{\partial z} = \left[\frac{1}{r}\frac{\partial}{\partial r}\left(rD_i(T)\frac{\partial n_i}{\partial r}\right) + \frac{\partial}{\partial z}\left(D_i(T)\frac{\partial n_i}{\partial z}\right)\right] + \left\{\frac{1}{r}\frac{\partial}{\partial r}\left(rD_i(T)\frac{\sigma_i e n_i}{k_b T}\frac{\partial\psi}{\partial r}\right) + \frac{\partial}{\partial z}\left[D_i(T)\frac{\sigma_i e n_i}{k_b T}\left(\frac{\partial\psi}{\partial z} - E\right)\right]\right\} \tag{23}$$

The following dimensionless parameters are introduced:

$$\bar{D}_i = \frac{D_i(T)}{D_{ref}} \qquad Pe = \frac{RU_{ref}}{D_{ref}} \qquad \bar{n}_i = \frac{n_i}{n_0} \qquad \bar{E} = \frac{R\sigma e E}{k_b T} \qquad \bar{t} = \frac{U_{ref}t}{R} \tag{24}$$

where D_{ref} is the reference ionic diffusion coefficient and Pe is the Péclet number, which gives the ratio of hydrodynamic convection to molecular diffusion. Generally, with small Péclet numbers (e.g., $Pe < 1$), the convection effects will be smaller than the ion diffusion effects, and the diffusion effect will be dominant; while with the large Péclet numbers (e.g., $Pe > 100$), the diffusion effect is negligible as compared to the convection. Using dimensionless parameters in eq 24, we can express the cationic and anionic concentration distributions in nondimensional form as

$$\frac{\partial\bar{n}_+}{\partial\bar{t}} + \bar{v}_r\frac{\partial\bar{n}_+}{\partial\bar{r}} + \bar{v}_z\frac{\partial\bar{n}_+}{\partial\bar{z}} = \frac{1}{Pe}\left[\frac{1}{\bar{r}}\frac{\partial}{\partial\bar{r}}\left(\bar{r}\bar{D}_+\frac{\partial\bar{n}_+}{\partial\bar{r}}\right) + \frac{\partial}{\partial\bar{z}}\left(\bar{D}_+\frac{\partial\bar{n}_+}{\partial\bar{z}}\right)\right] + \frac{1}{Pe}\left\{\frac{1}{\bar{r}}\frac{\partial}{\partial\bar{r}}\left(\bar{r}\bar{D}_+\bar{n}_+\frac{\partial\bar{\psi}}{\partial\bar{r}}\right) + \frac{\partial}{\partial\bar{z}}\left[\bar{D}_+\bar{n}_+\left(\frac{\partial\bar{\psi}}{\partial\bar{z}} - \bar{E}\right)\right]\right\} \tag{25a}$$

$$\frac{\partial\bar{n}_-}{\partial\bar{t}} + \bar{v}_r\frac{\partial\bar{n}_-}{\partial\bar{r}} + \bar{v}_z\frac{\partial\bar{n}_-}{\partial\bar{z}} = \frac{1}{Pe}\left[\frac{1}{\bar{r}}\frac{\partial}{\partial\bar{r}}\left(\bar{r}\bar{D}_-\frac{\partial\bar{n}_-}{\partial\bar{r}}\right) + \frac{\partial}{\partial\bar{z}}\left(\bar{D}_-\frac{\partial\bar{n}_-}{\partial\bar{z}}\right)\right] - \frac{1}{Pe}\left\{\frac{1}{\bar{r}}\frac{\partial}{\partial\bar{r}}\left(\bar{r}\bar{D}_-\bar{n}_-\frac{\partial\bar{\psi}}{\partial\bar{r}}\right) + \frac{\partial}{\partial\bar{z}}\left[\bar{D}_-\bar{n}_-\left(\frac{\partial\bar{\psi}}{\partial\bar{z}} - \bar{E}\right)\right]\right\} \tag{25b}$$

Boltzmann Distribution. Alternatively, for a symmetric electrolyte, the ionic concentration distributions are assumed to follow the Boltzmann distribution,

$$n_+ = n_0 e^{-\sigma e\psi/k_b T} \qquad n_- = n_0 e^{\sigma e\psi/k_b T} \tag{26}$$

With the use of the dimensionless parameters defined in eq 24, eq 26 can also be nondimensionalized as

$$\bar{n}_+ = e^{-\bar{\psi}} \qquad \bar{n}_- = e^{\bar{\psi}} \tag{27}$$

II.E. Initial and Boundary Conditions. The previously presented equations, including eqs 5, 9, 10, and 25, are subject to the following initial and boundary conditions: initial conditions ($\bar{t} = 0$),

$$\bar{v}_z = 0 \qquad \bar{v}_r = 0 \qquad \bar{n}_+ = 1.0 \qquad \bar{n}_- = 1.0 \qquad \bar{T} = 1.0 \tag{28a}$$

and boundary conditions at the inlet ($\bar{z} = 0$),

$$\bar{T} = 1.0 \qquad \bar{\psi} = 0 \qquad \frac{\partial \bar{v}_z}{\partial \bar{z}} = 0 \qquad \frac{\partial \bar{v}_r}{\partial \bar{z}} = 0$$
$$\bar{n}_+ = 1.0 \qquad \bar{n}_- = 1.0 \quad (28b)$$

For the channel length assumed to be sufficiently long, the flow is fully developed at the outlet ($\bar{z} = L/R$), and, hence, the outlet boundary conditions can be expressed as

$$\frac{\partial^2 \bar{t}}{\partial \bar{z}^2} = 0 \qquad \frac{\partial \bar{\psi}}{\partial \bar{z}} = 0 \qquad \frac{\partial \bar{v}_z}{\partial \bar{z}} = 0 \qquad \frac{\partial \bar{v}_r}{\partial \bar{z}} = 0$$
$$\frac{\partial \bar{n}_+}{\partial \bar{z}} = 0 \qquad \frac{\partial \bar{n}_-}{\partial \bar{z}} = 0 \quad (28c)$$

Because of the symmetry, the boundary conditions at the cylinder centerline ($\bar{r} = 0$) are

$$\frac{\partial \bar{T}}{\partial \bar{r}} = 0 \qquad \frac{\partial \bar{\psi}}{\partial \bar{r}} = 0 \qquad \frac{\partial \bar{v}_z}{\partial \bar{r}} = 0 \qquad \bar{v}_r = 0$$
$$\frac{\partial \bar{n}_+}{\partial \bar{r}} = 0 \qquad \frac{\partial \bar{n}_-}{\partial \bar{r}} = 0 \quad (28d)$$

At the capillary wall ($\bar{r} = 1$),

$$\bar{\psi} = \bar{\zeta} \qquad \bar{v}_z = 0 \qquad \bar{v}_r = 0 \qquad n_+ = e^{-\bar{\zeta}}$$
$$n_- = e^{\bar{\zeta}} \quad (28e)$$

where $\bar{\zeta}$ is the dimensionless zeta potential defined as $\bar{\zeta} = \sigma e \zeta / k_b T$.

In general, the temperature at the inner capillary wall is unknown. Because the heat generated by Joule heating and viscous dissipation in the electrolyte solution is mainly dissipated through the capillary wall to the surrounding environment, a conjugate heat transfer problem has to be solved to simultaneously account for the heat transfer in both the solution and the capillary wall.[18] The governing equation for heat conduction in the capillary wall is expressed as

$$\frac{\partial \bar{T}_s}{\partial \bar{t}} = \frac{1}{Pr\, Re}\left[\frac{1}{\bar{r}}\frac{\partial}{\partial \bar{r}}\left(\bar{r}\bar{k}_s\frac{\partial \bar{T}_s}{\partial \bar{r}}\right) + \frac{\partial}{\partial \bar{z}}\left(\bar{k}_s\frac{\partial \bar{T}_s}{\partial \bar{z}}\right)\right] \quad (29a)$$

where $\bar{T}_s$ is the dimensionless temperature of the capillary wall and $\bar{k}_s$ is the dimensionless thermal conductivity of the glass capillary.

The coupling boundary conditions are applied to the inner wall of the capillary

$$\bar{r} = 1 \qquad \bar{T}_s = \bar{T} \qquad -\bar{k}_s\frac{\partial \bar{T}_s}{\partial \bar{r}} = -\bar{k}_l\frac{\partial \bar{T}}{\partial \bar{r}} \quad (29b)$$

The third kind of temperature boundary condition is assumed at the outer channel wall,

$$-\bar{k}_s\frac{\partial \bar{T}_s}{\partial \bar{r}}\bigg|_{\bar{r}=1+\delta/R} = \frac{hR}{k_{ref}}(\bar{T}_s - 1) \quad (29c)$$

where δ is the thickness of the capillary wall and h is the heat transfer coefficient outside the capillary.

II.F. Mass Species Transport Equation. Because EOFs are usually used for injection and separation of biological or chemical samples such as DNA sequencing in genetic engineering,[3] another objective of this study is to evaluate the effect of Joule heating on the transport of sample species.

Consider a sample species to be transported between two reservoirs through a capillary filled with an electrolyte solution. For analysis, assumptions are made for no adsorption of the sample species onto the capillary wall and no interaction between the sample species and the electrolyte components. As the species transported by electrokinetic means in general is accomplished by three mechanisms, including hydrodynamic convection, diffusion, and electrophoresis, the mass-transport equation can be formulated as[1]

$$\frac{\partial C_i}{\partial t} + (v_z + u_{zi})\frac{\partial C_i}{\partial z} + (v_r + u_{ri})\frac{\partial C_i}{\partial r} = \frac{1}{r}\frac{\partial}{\partial r}\left[rD_{si}(T)\frac{\partial C_i}{\partial r}\right] +$$
$$\frac{\partial}{\partial z}\left[D_{si}(T)\frac{\partial C_i}{\partial z}\right] \quad (30)$$

where C_i is the ith sample species concentration, $D_{si}(T)$ is the temperature-dependent mass diffusivity of the ith sample species, and the dependence of $D_{si}(T)$ on T is assumed the same as that of $D_i(T)$ given in eq 22. u_{zi} and u_{ri} are the components of the electrophoretic velocity along the axial and radial directions, respectively. Conceptually, the electrophoretic velocity refers to the motion of a charged species in response to an applied electric field, and it is 0 for a neutral species.

Introducing the dimensionless parameters

$$\bar{C}_i = \frac{C}{C_{iref}} \qquad \bar{t}^* = \frac{t}{R^2/\nu} \qquad \bar{u}_{zi} = \frac{u_{zi}}{U_{ref}}$$
$$\bar{u}_{ri} = \frac{u_{ri}}{U_{ref}} \qquad \bar{D}_{si} = \frac{D_{si}(T)}{D_{s\,ref}}$$
$$Sc = \frac{\nu_{ref}}{D_{s\,ref}} \quad (31)$$

Then, eq 30 can be nondimensionalized as

$$\frac{\partial \bar{C}_i}{\partial \bar{t}^*} + Re(\bar{v}_z + \bar{u}_{zi})\frac{\partial \bar{C}_i}{\partial \bar{z}} + Re(\bar{v}_r + \bar{u}_{ri})\frac{\partial \bar{C}_i}{\partial \bar{r}} =$$
$$\frac{1}{Sc}\left[\frac{1}{\bar{r}}\frac{\partial}{\partial \bar{r}}\left(\bar{r}\bar{D}_{si}\frac{\partial \bar{C}_i}{\partial \bar{r}}\right) + \frac{\partial}{\partial \bar{z}}\left(\bar{D}_{si}\frac{\partial \bar{C}_i}{\partial \bar{z}}\right)\right] \quad (32)$$

where C_{iref} and $D_{s\,ref}$ are respectively the reference concentration and the mass diffusivity of the ith species and Sc is the Schmidt number. The initial and boundary conditions are

$$\bar{t}^* = 0 \quad \bar{C}_i = 0.0 \quad (33a)$$

inlet: $$\bar{C}_i = 1.0 \quad (33b)$$

outlet: $$\frac{\partial^2 \bar{C}_i}{\partial \bar{z}^2} = 0 \quad (33c)$$

symmetry centerline: $$\frac{\partial \bar{C}_i}{\partial \bar{r}} = 0 \quad (33d)$$

capillary wall: $$\frac{\partial \bar{C}_i}{\partial \bar{r}} = 0 \quad (33e)$$

III. Numerical Method

Because the thermophysical coefficients are temperature-dependent, the formulated equations, including eqs

3, 9, 10, 18, and 25, are strongly coupled, and, hence, they must be solved iteratively using the CFD technique. The numerical scheme used to solve the proposed mathematical models is based on the finite volume method.[24] The previously derived equations are discretized using the control volume integration. The nonlinear source terms are linearized using the Taylor's series expansion. The pressure−velocity coupling in the Navier−Stokes equation is solved using the Semi-Implicit Method for Pressure Linked Equations.[24] To solve the discrete algebraic equations, the line-by-line Tridiagonal Matrix Algorithm scheme is employed. In the calculation, the coupled ionic concentration distributions, electrical potential profiles, and velocity and temperature fields are computed first, and then the species concentration distributions in the microcapillary are calculated according to eq 32. In addition, because the electrokinetic radius, κR, used in the case studies varies by several orders of magnitude, including 16, 500, and 5000 for comparing the Nernst−Planck equation and the Boltzmann distribution and 75 000 for computing Joule heating and its effects, a grid-independent study is carried out for each case to ensure that the chosen grid system can produce grid-independent solutions.

IV. Results and Discussion

IV.A. Nernst−Planck Equation Versus the Boltzmann Equation. As mentioned earlier, the ionic concentration distributions, in general, are governed by the Nernst−Planck equation, while in most cases the Boltzmann distribution is assumed to describe the ionic concentration distributions because of its simplicity. However, in the literature, no study has been reported to quantitatively compare the ionic concentration distributions obtained from these two models. A systematic study is, therefore, carried out to evaluate the ionic concentration distributions in both the developing and the fully developed EOF regions on the basis of the Nernst−Planck equation and the Boltzmann distribution. Meanwhile, the results of the EOF velocity field and temperature field (produced by Joule heating) are also presented.

In the calculations, κR is selected as 16, 500, and 5000, corresponding to a capillary of 10 μm in diameter and electrolyte ionic concentrations of 10^{-6}, 10^{-3}, and 10^{-1} M, respectively. The microcapillary is made from silica glass and has a length of $L = 50$ mm and a wall thickness of $\delta = 70$ μm (Polymicro Technologies, U.S.A.). The working fluid is NaCl solution, and its properties are density $\rho = 998$ kg/m^3, electric conductivities at room temperature (298 K) $\lambda_{+0} = 50.08 \times 10^{-4}$ m^{2}S/mol and $\lambda_{-0} = 76.31 \times 10^{-4}$ m^{2}S/mol, and ionic diffuse coefficients at room temperature $D_{+0} = 1.334 \times 10^{-9}$ m^2/s and $D_{-0} = 2.032 \times 10^{-9}$ m^2/s.

Ionic Concentration Distribution. Figure 2a−c shows the steady-state radial distributions of dimensionless concentration (with respect to the bulk ionic concentration) for the co-ions and counterions at various axial locations when (a) $\kappa R = 16$, (b) $\kappa R = 500$, and (c) $\kappa R = 5000$, corresponding to the cases shown in Figure 2a−c, respectively. From the EDL theoretical viewpoint, the diffuse layer of the EDL (or the extent of the EDL) is defined as such a regime in which there are more counterions than co-ions and, hence, the net charge density is not 0. Therefore, the dependence of the EDL regime and the development of the EDL in the presence of the flow on the electrokinetic diameter can be reflected from the radial distributions of the co-ions and counterions. It is noted from Figure 2a that, at the inlet region (i.e., small z/R values), the EDL (i.e., the regime where variation of ionic

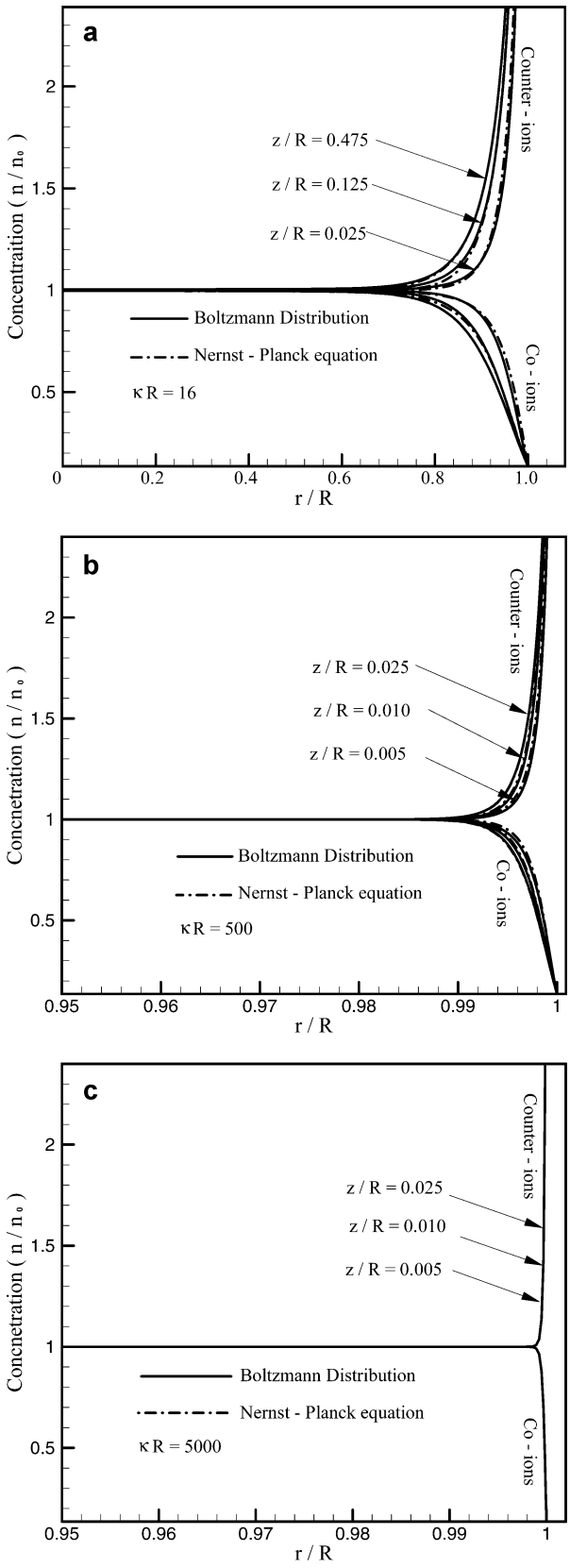

Figure 2. Steady-state radial distributions of dimensionless ionic concentration for both co-ions and counterions at various axial locations predicted by the Nernst−Planck equation and the Boltzmann distribution; other parameters used in the computation are $E = 500$ V/cm, $\zeta = -50$ mV, and $h = 10$ W/(m^2 K). (a) $\kappa R = 16$, (b) $\kappa R = 500$, and (c) $\kappa R = 5000$.

(24) Patankar, S. V. *Numerical Heat Transfer and Fluid Flow*; McGraw-Hill: New York, 1980.

concentrations occurs) forms only in a very thin layer close to the capillary wall. As the flow develops (i.e., large z/R values), the variation of ion concentrations gradually extends to the center region of the capillary, indicating the EDL regime is getting larger with flow developing. Further, a comparison among Figure 2a−c indicates that the EDL regime reduces as the electrokinetic diameter, κR, increases.

Although Figure 2a−c shows that the ionic concentration spatial development patterns predicted by the Nernst−Planck equation and the Boltzmann distribution are similar, the difference of the two models and the effect of the electrokinetic radius κR on the concentration distributions are clearly demonstrated. It can be seen that when the electrokinetic radius is small, for example, $\kappa R = 16$, the radial distributions of ionic concentration obtained from the Nernst−Planck equation are different from those obtained from the Boltzmann equation within the entrance region (e.g., $z/R \leq 0.475$ when $\kappa R = 16$). Beyond such an entrance region, no difference can be observed. As pointed out earlier, such difference occurring in the entrance region should be attributed to the flow development. When the electrokinetic radius is increased to $\kappa R = 500$, the influence of the EOF on the ionic concentration distributions reduces. As such, the entry region, in which the ionic concentration distributions obtained from the Nernst−Planck equation and the Boltzmann distribution are different, becomes smaller (see Figure 2b). Further increment of the electrokinetic radius to $\kappa R = 5000$ makes the EDL become so thin that the effect of the EOF on the ionic concentration distributions inside the EDL regime is negligible. Therefore, as indicated in Figure 2c, the difference of the co-ion and counterion distributions calculated by the Nernst−Planck equation and the Boltzmann distribution is virtually indistinguishable.

In our cases, the typical Reynolds number is on the order of 10^{-2}. For the ions in the electrolyte, the Schmidt number is smaller than 10^2, and, hence, the Péclet number ($Sc\,Re$) is smaller than 1, suggesting that the contribution to the ionic concentration distributions due to hydrodynamic convection is smaller than that due to molecular diffusion. Because the major difference between the Nernst−Planck equation and the Boltzmann distribution lies in that the former takes care of the effect due to the hydrodynamic flow, both models would give similar results of the ionic concentration distributions for the conditions considered in the case study.

Velocity Field. Figure 3a−c respectively shows the steady-state radial distributions of dimensionless axial velocity [with respect to the reference velocity defined by using the Smoluchowski velocity [$U_{ref} = (\epsilon_{ref}\epsilon_0/\mu_{ref})E\zeta$] at various axial locations when (a) $\kappa R = 16$, (b) $\kappa R = 500$, and (c) $\kappa R = 5000$. Other parameters used in the computation are $E = 500$ V/cm, $\zeta = -50$ mV, and $h = 10$ W/m^{2}K. According to eq 10a,b, the EOF is induced by the interplay of the imposed electric field and the net charge density (defined in eq 2 and related to the difference between counterions and co-ions within the EDL). Because the applied electric field strength is kept constant, the EOF velocity field is mainly determined by ionic concentration distributions. Hence, the effect of κR on the velocity distributions obtained from the two models exhibits the same tendency as that on the ionic concentration distributions shown in Figure 2a−c. For small κR (e.g., $\kappa R =$ 16 and 500), the EOF velocity distributions shown in Figure 3a,b predicted by the Nernst−Planck equation are different from those obtained from the Boltzmann distribution in the developing region, and such a difference

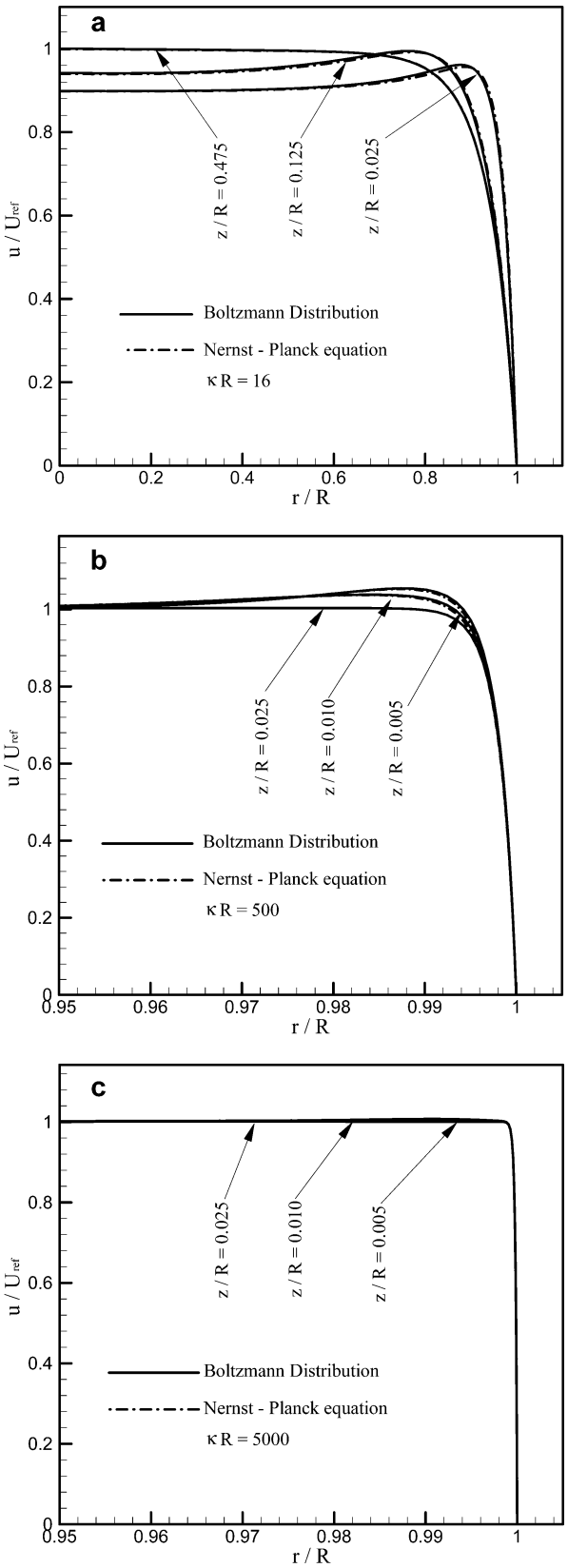

Figure 3. Steady-state EOF velocity distributions at various axial locations predicted by the Nernst−Planck equation and the Boltzmann distribution; other parameters used in the computation are $E = 500$ V/cm, $\zeta = -50$ mV, and $h = 10$ W/(m^2 K). (a) $\kappa R = 16$, (b) $\kappa R = 500$, and (c) $\kappa R = 5000$.

gradually disappears as κR increases. For very large κR, for example, $\kappa R = 5000$, the velocity distributions calculated by the Nernst−Planck equations approach the results predicted by the Boltzmann distribution.

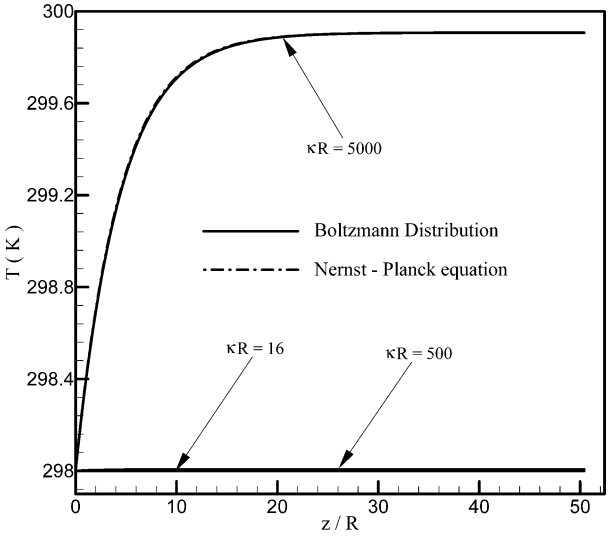

Figure 4. Steady-state mean temperature profiles of electrolyte solution along the axial direction for three different values of the electrokinetic radius, κR; other parameters used in the computation are $E = 500$ V/cm, $\zeta = -50$ mV, and $h = 10$ W/(m^2 K).

In addition, when the EDL thickness is comparable to the capillary radius, for example, $\kappa R = 16$, one can observe (from Figure 3a) how the EOF velocity develops spatially; it is in a fashion similar to the spatial development of the EDL. In the developing region, it is found that the velocity reaches the highest at a position near the capillary wall and then gradually falls toward the capillary centerline. This scenario reveals the nature of the EOF; the driving force of the EOF only exists within the EDL regime, where the net charge density is not 0. The flow outside of the EDL regime in the capillary is attributed to hydrodynamic shear stress due to viscosity. Similar findings were also reported by Yang et al.[20]

Temperature Profile. Variation of the steady-state mean temperature profiles of the electrolyte along the axial direction for three different values of the electrokinetic radius, κR, is shown in Figure 4. It is noted that, for the lower values of κR, such as $\kappa R = 16$ and 500, the solution temperature virtually keeps flat. This suggests in the cases of dilute electrolyte concentrations (e.g., less than 10^{-3} M) or small capillary sizes (e.g., 10 μm in diameter), the Joule heating is negligible, while for higher values of κR (e.g., 5000 or more), the Joule heating can be observed. However, the results of the mean temperature profile show no difference between the Nernst−Planck equation and the Boltzmann distribution. This is expected because in the case of $\kappa R = 5000$, both the Nernst−Planck equation and the Boltzmann distribution give the same results for both the ionic concentration distribution and the velocity field. Therefore, according to eq 18, the results of the temperature profiles obtained from the Nernst−Planck equation and the Boltzmann distribution should be same.

From a practical viewpoint, the CE is usually used to handle buffer solutions of at least 10^{-2} M in a capillary of 100 μm in diameter, which corresponds to $\kappa R > 10\,000$. Therefore, on the basis of the results presented in Figures 2a−c, 3a−c, and 4, it can be concluded that, as the Joule heating is concerned, the simple Boltzmann distribution is adequate in lieu of the general Nernst−Planck equation for estimation of the ionic concentration distribution and, hence, the EOF velocity field.

IV.B. Transient Joule Heating and Its Effects. In this section, the Joule heating and its effects on the EOF and sample species transport are discussed. On the basis of the conclusion drawn in the previous section, the results presented in this section are obtained using the Boltzmann distribution. The DNA species is chosen as the sample transport in the microcapillary. According to Ohara et al.,[25] the DNA mass diffusivity and electrophoretic mobility (at room temperature) are $D_{si0} = 2.03 \times 10^{-11}$ m^2/s and $u_{zi0} = u_{ri0} = 2.74 \times 10^{-8}$ m^2/(V s), respectively.

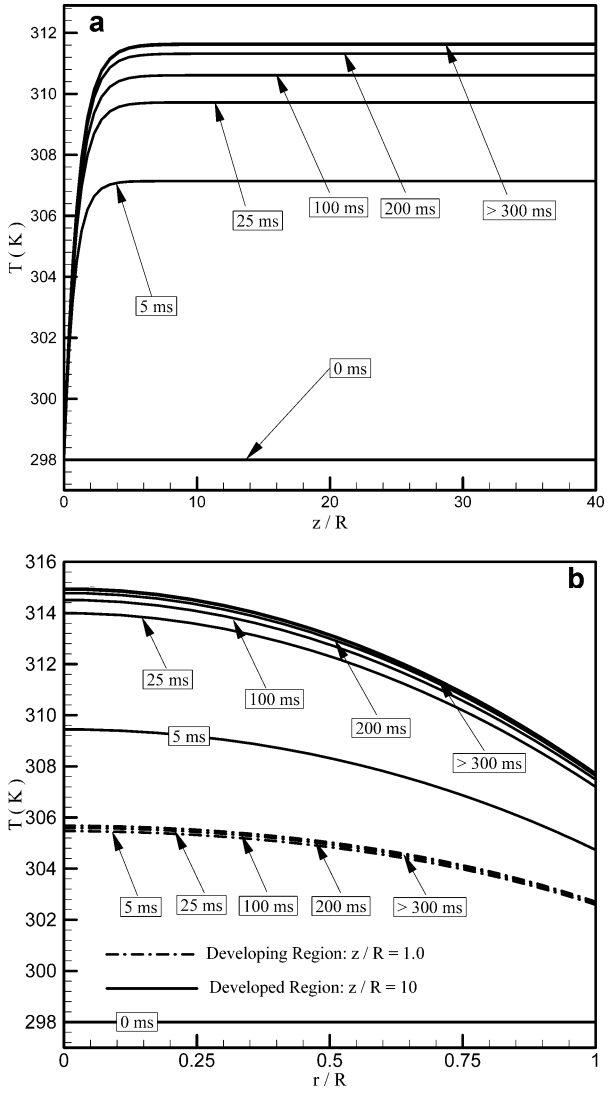

Figure 5. Temporal and spatial developments of the Joule heating induced solution temperature field in a microcapillary with the following parameters: $R = 75$ μm, $E = 500$ V/cm, $C = 0.1$ M, $\zeta = -50$ mV, and $h = 10$ W/(m^2 K). (a) Variation of the mean temperature along the axial direction. (b) Radial temperature distributions in both the developing and the developed regions.

Temperature Development Due to the Joule Heating. Figure 5a,b respectively shows the time evaluation of the axial mean temperature profiles and the radial temperature distributions of a liquid solution in a capillary with the following parameters: capillary inner radius $R = 75$ μm, applied electric field $E = 500$ V/cm, bulk concentration $C = 0.1$ M, zeta potential $\zeta = -50$ mV, and heat transfer coefficient outside the capillary wall $h = 10$ W/(m^2 K). The development of the solution temperature due to the Joule heating in both thermal developing and developed regions is clearly demonstrated in these two figures. It is found that the solution temperature starts at the room tem-

(25) Ohara, T.; Torii, D.; Majumdar, A.; Dunphy, K. *The 6th ASME-JSME Thermal Engineering Joint Conference* **2003**, TED-AJ03-406.

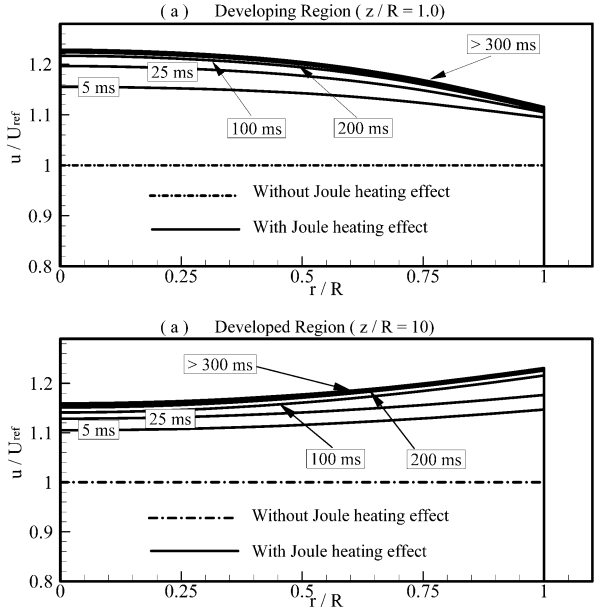

Figure 6. Time evolution of the EOF velocity radial distributions in (a) the developing region and (b) the fully developed region with and without the Joule heating effect. The parameters used in the computation are $R = 75\ \mu$m, $E = 500$ V/cm, $C = 10^{-1}$ M, $\zeta = -50$ mV, and $h = 10$ W/(m^2 K).

perature at the entrance and achieves a fully developed temperature after a 3−5 radii distance along the axial direction. Interestingly, the thermal entrance region (or developing length) is independent of time. Furthermore, the results show that the time for the temperature field to attain the steady state is very short at the inlet and then gradually increases in the thermal developing region. While in the thermal developed region, the Joule heating starts to heat up the liquid solution very fast at the initial stage. Subsequently, the solution temperature gradually increases as the time elapses and finally reached its steady state at 300 ms after the electric field is set up.

Joule Heating Effect. Figure 6 shows the transient dimensionless velocity distributions of the EOF in both the developing and the developed regions. As a comparison, the EOF velocity without consideration of Joule heating is also plotted as dotted lines. According to Kang et al.,[5] without the Joule heating effect the EOF can attain its steady state instantly upon imposing the electric field (the characteristic time for the EOF to reach its steady state is estimated as $t_{cr} = R^2/\nu = 5$ ms in this case), and because of large κR, the dimensionless EOF velocity approaches the Smoluchowski velocity. With consideration of the Joule heating effect, however, it is found that the time for the EOF to reach its steady state significantly increases to 300 ms. It is also interesting to note that the EOF development time is almost the same as that of the temperature field development (as shown in Figure 5a,b). This suggests that the change of the velocity distributions is mainly caused by the change of solution temperature resulted from the Joule heating, and the EOF field becomes strongly coupled with the Joule heating induced temperature field. The influence of temperature on the EOF velocity is attributed to the dependence of the solution viscosity on the temperature. Therefore, under the Joule heating effect, the increment of the solution temperature causes a decrease in the solution viscosity and dielectric constant and, hence, results in the dimensionless EOF velocity larger than the reference Smoluchowski velocity.

The steady-state axial velocity vectors with and without the Joule heating effect in both the developing and the developed regions are presented in Figure 7. It is found that as a result of a large κR, the entrance effect on the EOF velocity distributions under no Joule heating effect is indiscernible. In contrast, the velocity distributions with the Joule heating effects in the developing and the fully developed regions exhibit very differently. The results show that the velocity distribution has a parabolic shape in the developing region, while with the flow advance it becomes flat and eventually reaches a slight concave pattern in the developed region. This scenario can be explained as follows. Because of the Joule heating, the solution mean temperature rises along the channel, as shown in Figure 5a. As discussed earlier, an increase in the temperature would reduce the solution viscosity and, hence, results in an increasing velocity. Consequently, as the flow develops from the entrance to the fully developed region, the EOF velocity increases. This would produce a "suction" effect (i.e., a favorable pressure gradient) on the developing flow and accordingly a "drag" effect (i.e., an adverse pressure gradient) to the developed flow. Our numerical results does show the existence of a small negative pressure gradient in the developing region and a positive pressure gradient in the fully developed region, and they are shown in Figure 8, which presents the variation of the pressure along the axial direction. In the literature, the effect of a favorable pressure gradient and adverse pressure gradient on EOF was discussed in length by Santiago.[26]

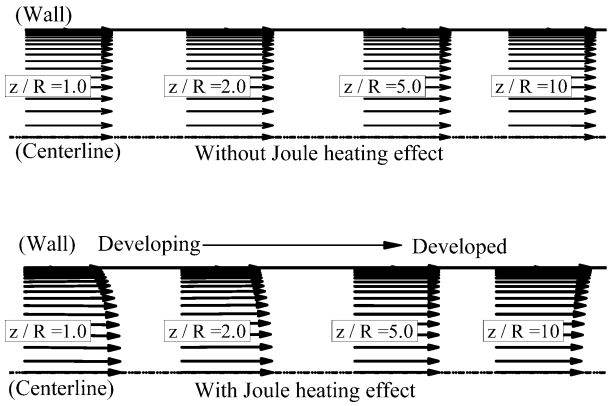

Figure 7. Steady-state EOF velocity vectors in both the developing and the fully developed regions with and without the Joule heating effect. The parameters used in the computation are $R = 75\ \mu$m, $E = 500$ V/cm, $C = 10^{-1}$ M, $\zeta = -50$ mV, and $h = 10$ W/(m^2 K).

The transport of the sample species in a capillary with and without the Joule heating effect is shown in Figure 9. Because of the low diffusion coefficient of the sample species (for DNA,[26] $D_i = 10^{-11}$ m^2/s), the Schmidt number for the DNA sample species is very larger (on the order of 10^4). As mentioned earlier, the typical Reynolds number in our case studies is on the order of 10^{-2}. Hence, we can estimate that the Péclet number $Pe = Re\ Sc$ is on the order of 10^2, suggesting that the diffusion of the sample species is negligible as compared to the convection. The species transport is dominated by convection and mainly transported with the flow. In the case of no Joule heating effect, it is noted that the sample transport exhibits nondispersion, which is a unique advantage of the electrokinetic transport mode adopted in the BioMEMS design. With including the Joule heating effect, it can be seen that the sample species transports faster than that without considering the Joule heating effect due to an increase of the electroosmotic velocity as shown in Figure

(26) Santiago, J. G. *Anal. Chem.* **2001**, *73*, 2353−2365.

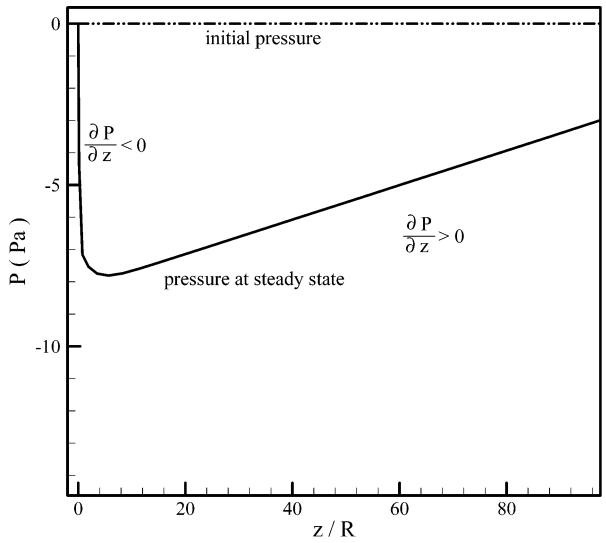

Figure 8. Variation of the pressure profiles along the axial direction. The parameters used in the computation are $R = 75$ μm, $E = 500$ V/cm, $C = 10^{-1}$ M, $\zeta = -50$ mV, and $h = 10$ W/(m^2 K).

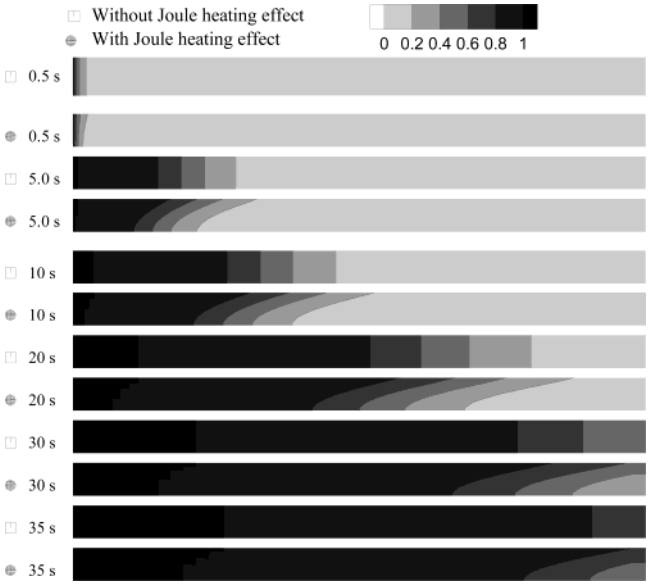

Figure 9. Time Evolution of the sample species concentration distributions in the capillary with and without the Joule heating effect. The parameters used in the computation are $R = 75$ μm, $E = 500$ V/cm, $C = 10^{-1}$ M, $\zeta = -50$ mV, and $h = 10$ W/(m^2 K).

6. Moreover, because the sample electrophoretic mobility increases with increasing temperature, the presence of a radial temperature gradient (shown in Figure 5b) gives rise to a variation of the sample axial electrophoretic mobility along the radial direction and, hence, results in the sample species being very dispersive. Because the direction of the electrophoretic velocity for negatively charged samples (e.g., DNA species) is opposite to that of the EOF velocity, it can be clearly observed from Figure 9 that the sample species in the central region is transported much slower than that close to the wall region, and such difference becomes larger as time elapses.

V. Conclusion

In this study, a mathematical model has been developed to evaluate the Joule heating and its effects on the temporal and spatial EOF developments and sample species electrokinetic transport. It is found for low values of κR where the EDL plays an important role, in the EOF developing region the ionic concentration distribution predicted by the Nernst−Planck equation deviates from the Boltzmann distribution. As the EOF develops, the deviation becomes smaller, and finally in the EOF fully developed region, the Nernst−Planck equation gives the ionic concentration distribution the same as the Boltzmann distribution. For large values of κR where the the EDL regime is thin compared to the capillary radius, the Nernst−Planck equation and the Boltzmann distribution predicts the identical ionic concentration distributions in both the developing and the developed regions of the EOF. These findings suggest that as the Joule heating is concerned where κR usually is large, the simple Boltzmann distribution can be assumed.

The simulations show that, as a result of the coupling between the EOF field and the temperature filed, the EOF has almost the same entrance length as the Joule heating induced temperature development. The Joule heating causes the development of radial and axial temperature distributions in the capillary, resulting in deviation of the EOF velocity from its normal profile. It is found that as a result of the Joule heating the EOF in the developing region exhibits a parabolic pattern, while in the fully developed region it has a concaved shape. In addition, the temperature increment and the presence of the temperature gradients make the sample species axially transport faster and more dispersive along the radial direction of the capillary.

Acknowledgment. Financial support from the Nanyang Technological University for the Academic Research Fund to C.Y. and the Ph.D. scholarship awarded to G.Y.T. are gratefully acknowledged.

LA0301994